ELSEVIER

Polymer 41 (2000) 4699–4707

polymer

Structure–property relationships for cyanurate-containing, full interpenetrating polymer networks

F.J. Balta Calleja[a,*], E.G. Privalko[b], D.I. Sukhorukov[b], A.M. Fainleib[b], L.M. Sergeeva[b], T.A. Shantalii[b], V.I. Shtompel[b], M. Monleon Pradas[c], G. Gallego Ferrer[c], V.P. Privalko[a,b]

[a]*Instituto de Estructura de la Materia, CSIC, Serrano 119, 28006 Madrid, Spain*
[b]*Institute of Macromolecular Chemistry, National Academy of Sciences of Ukraine, 253160 Kiev, Ukraine*
[c]*Universidad Politecnica de Valencia, P.O. Box 22012, E-46071 Valencia, Spain*

Received 25 February 1999; accepted 9 July 1999

Abstract

Full sequential interpenetrating polymer networks (seq-IPN) of cross-linked polyurethane (CPU) and heterocyclic polymer networks (HPN) based on thermally cured dicyanic ether of Bisphenol A (DCE) were characterized by small-angle X-ray diffraction, dynamic mechanical analysis, stretching calorimetry and microhardness measurements. Neat CPU was shown to be a microphase-separated system characterized by a regular, three-dimensional macrolattice of network junctions, embedded in uniform-size microdomains of stiff chain fragments which spanned the continuous matrix of soft chain fragments. In contrast, no large-scale structural heterogeneities were detected in the HPN. The X-ray long spacing (L), the degree of microphase segregation (DMS), the α-relaxation temperature and the mechanical properties (elastic modulus and microhardness) were studied as a function of HPN content. Results are explained in the light of a model that discusses the maximum degree of CPV swelling by molten DCE as a function of composition. It is suggested that predominantly chemical interactions between the molten DCE and the stiff chain fragment microdomains, reinforcing primary physical interactions, are responsible for the observed transition at 40% HPN content to a more homogeneous phase morphology of seq-IPNS. © 2000 Published by Elsevier Science Ltd. All rights reserved.

Keywords: Full, Sequential IPN; Structural heterogeneity

1. Introduction

Heterocyclic polymer networks (HPNs) produced by polycyclotrimerization of dicyanates, diisocyanates, etc. exhibit a number of advantages including excellent chemical resistance, low dielectric losses and good adhesion to metals [1–5]. However, the mechanical performance of HPNs under conditions of shock loading is rather poor. A possible way to improve the impact properties of HPNs could be the preparation of full or semi-interpenetrating polymer networks (IPNs) from an HPN and an appropriately chosen elastic polymer component [6–8]. In preceding publications [9–12], two series of semi-IPNs based on the same linear polyurethane and two different HPNs, respectively, were characterized by small-angle X-ray scattering, calorimetry, dynamic mechanical analysis and microhardness measurements.

The aim of the present paper is to extend the above investigations to the study of structure–property relationships for a series of full, sequential IPNs based on a cross-linked polyurethane and an HPN.

2. Experimental

2.1. Materials

Full, sequential IPN (seq-IPN) were obtained by the standard procedure. The network component 1 (cross-linked polyurethane, CPU) prepared at the first stage was then swollen in a molten dicyanic ether of Bisphenol A (DCE), and the latter was thermally cured at the second stage to produce the network component 2 (HPN).

Stage 1. Prior to reaction, the oligoether (oligotetramethylene glycol, molar mass 1 kg/mol) was dehumidized by heating to 353 K and evacuation at 10 mm/Hg. Thereafter, the oligoether was mixed with 70% solution, in ethylacetate of the adduct of glycerol and 2,4-toluene diisocyanate, and the mixture was evacuated for a duration of 1 h at room temperature to remove the solvent. The

* Corresponding author.

0032-3861/00/$ - see front matter © 2000 Published by Elsevier Science Ltd. All rights reserved.
PII: S0032-3861(99)00504-2

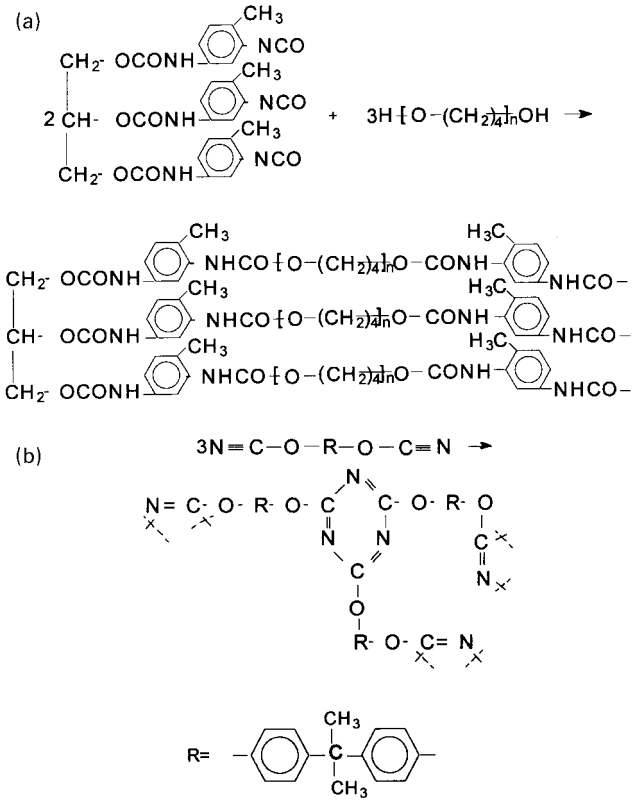

Fig. 1. Reaction schemes for: (a) the synthesis of CPU and (b) for curing of DCE.

solvent-free mixture was sandwiched between two glass plates and finally cured by heating to 353 K and subsequent isothermal storage for a duration of 8 h to produce the 1-mm thick film of the CPU (Fig. 1a). The cure completion was checked by monitoring the disappearance of the IR absorption band at 2270 cm^{-1} characteristic to isocyanate groups [13].

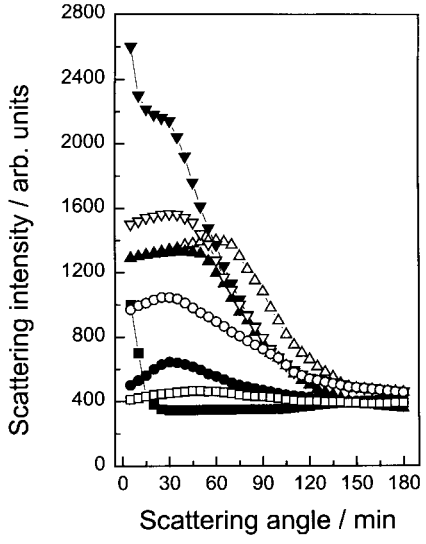

Fig. 2. SAXS curves for CPU (△) and HPN (■), and for seq-IPN with the following CPU/HPN compositions: 89/11 (▲), 86/14 (▼), 82/18 (▽), 65/35 (○), 55/45 (●) and 42/52 (□).

Stage 2. Full seq-IPNs with different HPN contents (determined from the weight gain after swelling) were prepared by swelling of CPU films in the molten DCE at 353 K and subsequent step-wise isothermal curing of the latter by storage, first, at 423 K for a duration of 5 h, and then at 453 K for a duration of 3 h. The degree of the DCE cure was checked by monitoring the intensity decrease (till complete disappearance) of the IR absorption band at 2272–2236 cm^{-1} (stretching vibrations of N≡C–O– groups) and concomitant appearance (and increase of intensity) of absorption bands at 1570 and 1370 cm^{-1} (vibrations of a cyanurate cycle) [13]. Presumably, the main structural entities in the HPN are thermally stable six-membered, three-arm triazine rings (Fig. 1b).

2.2. Techniques

Small-angle X-ray scattering (SAXS) profiles were obtained with a Kratky camera (KRM-type diffractometer). The primary beam intensity was controlled with a monitoring channel in the scattering range between 3′ and 5° (2Θ). Cu K_α radiation and nickel filtering of the primary beam were used. Recording of the scattering radiation with a scintillation counter and digital conversion was performed using the step-by-step scanning regime. The geometrical parameters of the X-ray beam in the specimen plane and the detector position were chosen so as to satisfy the conditions of an "infinite" slit collimation (30 mm for the length of the homogeneous portion of X-ray beam and 290 mm for the specimen–detector distance). The absolute scattering intensity of the samples was determined by calibrating the instrument with a standard Kratky sample of Lupolen [14,15]. The mean interdomain spacing ("long periods"), L, was calculated using Bragg's equation.

The dynamic elastic modulus E' and the mechanical loss tangent (tan δ) were measured with a dynamic mechanical thermal analyzer (Seiko DMS 210), n the temperature interval 130–625 K (loading mode: tension; frequency: 1 Hz; heating rate: 2 deg/min).

The mechanical work (W) and concurrent heat effects (Q) in the step-wise loading (stretching)/unloading (contraction) cycles were measured (with the estimated mean error below 2%) at room temperature with the stretching calorimeter described in detail elsewhere [16–19]. In a typical run, each specimen was stretched at a constant velocity q^+ to a predetermined strain ϵ_i, stored at fixed ϵ_i to the full completion of mechanical and thermal relaxations, and, thereafter, allowed to contract at the same velocity q^- to zero force. The typical difference between fixed strains in two successive steps, $\epsilon_{i+1} - \epsilon_i$, varied from several digits in the fourth place to a few digits in the third place within the strain intervals below and above 0.02, respectively.

A Leitz Tester equipped with a square-based diamond indenter was used for the room-temperature microhardness

Table 1
Properties of seq-IPNs

CPU/HPN	T_α (K)	E (GPa)	$10^5 \times \alpha_L$ (K^{-1})	H (MPa)
100/0	365	0.20	18.4	43.6
88/12	360	0.26	10.0	31.6
78/22	375	0.52	6.1	63.6
62/38	405	1.10	5.3	178.1
51/49	435	2.60	4.0	247.1
37/63	455/540	3.50	3.2	236.2
0/100	485/570	4.05	2.2	241.7

(H) measurements. The H-values were calculated from the standard equation [19,20] $H = kS$ (MPa), where S is the slope of the straight-line plot of the residual projected indentation area $A(m^2) = d^2$ vs. the contact load applied P (in Newton), d (in meter) is the diagonal length of the impression, and $k = 1.854$ is the geometrical factor. In a loading cycle of 0.1 min the loads of 0.5, 1 and 1.5 N were used. For each point, at least 3–5 measurements were averaged. The correlation coefficients and the standard deviations for the linear A vs. P fits obtained were 0.994–0.998 and 1.40–1.16, respectively.

3. Results and discussion

3.1. Phase morphology

The occurrence of a distinct SAXS reflection for the neat CPU (Fig. 2) supports the concept of a regular, three-dimensional macrolattice of network junctions embedded in uniform-size microdomains of stiff chain fragments (STF) which span the continuous matrix of soft chain fragments (SFT). In contrast, the smooth decay of the SAXS curve for the neat HPN suggests the absence of large-scale structural heterogeneities.

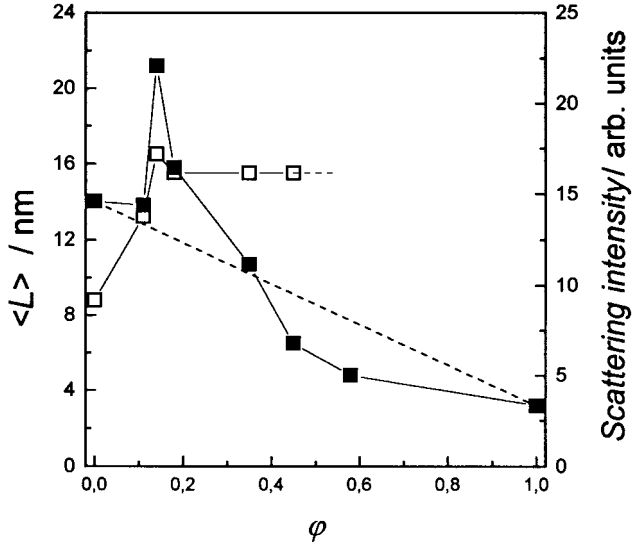

Fig. 3. Composition dependence of long spacing (□) and SAXS peak intensity (■).

In the case of seq-IPNs, one can distinguish among three composition intervals to describe the behavior of the long period (cf. Table 1 and Fig. 3): (1) an initial sharp (nearly two-fold) increase of L at small HPN content ($\varphi \leq 0.15$); (2) a constancy of L in the intermediate composition range (up to $\varphi \leq 0.5$); (3) an absence of clear-cut SAXS reflections for $\varphi \geq 0.5$. The SAXS peak intensity (which can serve as an indirect measure of the degree of microphase segregation, DMS [14,15,21]) changes in a non-additive fashion with the seq-IPN composition (Fig. 3), exhibiting large positive deviations from linear additivity (broken line in Fig. 3) in the interval $\varphi \leq 0.4$, and negative deviations at higher HPN contents.

These results can be explained as follows: in the range $\varphi \leq 0.15$, the sudden increase of L from $L_{CPU} = 8.8$ nm, for the initial neat CPU, up to $L_{IPN} = 16.5$ nm for the corresponding seq-IPN, and the concurrent "overshoot" of the SAXS peak intensity above the additivity value are in favor of: (a) an homogeneous swelling of the continuous soft matrix of CPU by molten DCE; and (b) an increased DMS of the resulting seq-IPN due to the subsequent formation of sharp interfaces between isolated inclusions of the HPN and the SFT-rich matrix of CPU, respectively.

The constancy of $L = 15.5$ nm in the composition interval ($0.15 < \varphi \leq 0.5$) suggests that the maximum degree of the CPU swelling, Q_{max}, is reached already in the first interval. Assuming $Q_{max} \approx (L_{IPN}/L_{CPU})^3 = (15.5/8.8)^3 = 5.5$, it can be readily seen that the volume increment of the swollen CPU exceeds, by far, the actual content of the HPN within corresponding seq-IPNs. Hence, it can be concluded that in the second composition interval, only a relatively small fraction (i.e. of the order of $\varphi \approx 0.15$) of the available molten DCE was in a direct interaction with the expanded SFT fragments of the CPU. On the other hand, the remaining DCE simply filled the empty space created by swelling. A similar argument was invoked [22] to explain the equilibrium swelling of polyurethane elastomers in more common solvents.

During the subsequent cure of the molten DCE, one could have anticipated the further increase of a structural heterogeneity of the seq-IPN due to the formation of a larger total interfacial area between cured components. However, the observed smooth decrease of the SAXS peak intensity below the additivity value (Figs. 2 and 3) is contrary to the expected trend. Apparently, the only reasonable explanation for the observed lowering of the DMS of seq-IPNs is the smearing out of the sharp interface between components due to strong chemical interactions of the excess of the DCE with unreacted functional groups at the periphery of STF-rich microdomains of the CPU. This hypothesis seems reasonable in view of the well known ability of cyanates for chemical interactions with compounds containing the active hydrogen [23]. Thus, the increased contribution of

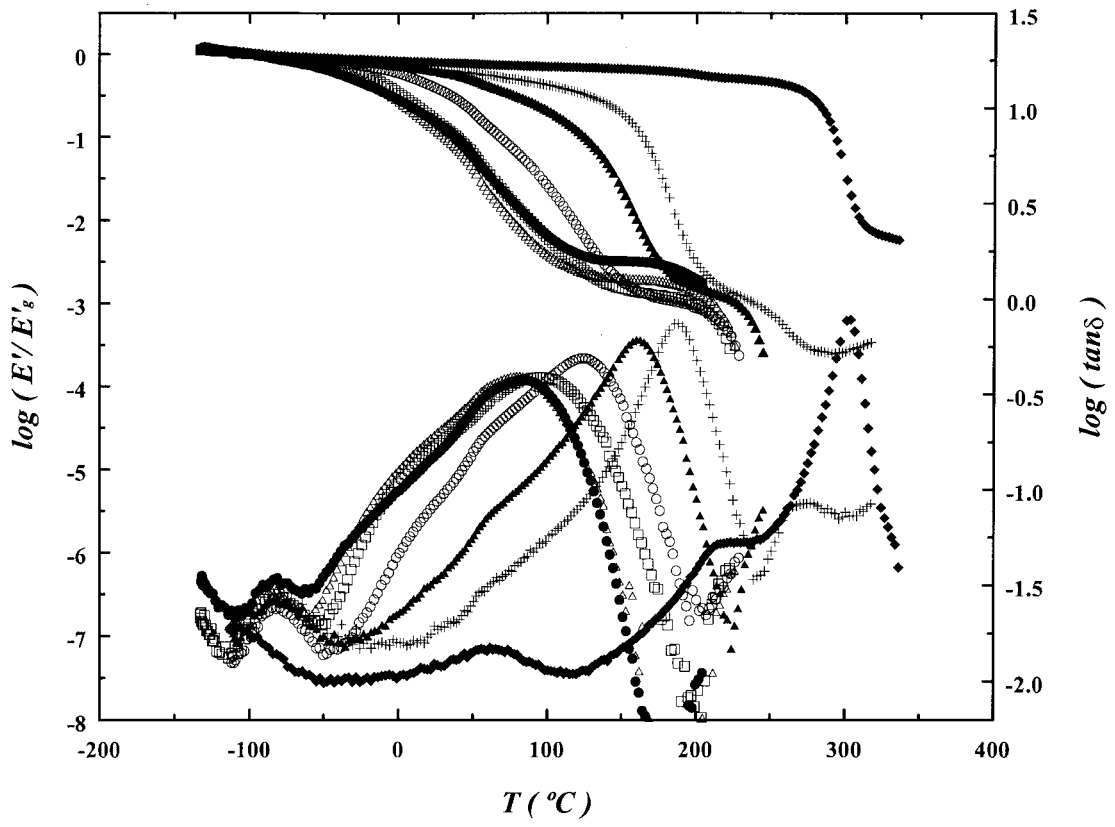

Fig. 4. Temperature dependence of the dynamic Young's modulus and of the mechanical loss tangent for CPU (●) and HPN (◆), and for seq-IPNs of the following CPU/HPN compositions: 88/12 (△), 78/22 (□), 62/38 (○), 51/49 (▲) and 37/63 (×).

such interactions is the most probable cause for the gradual decrease of the DMS of seq-IPNs (eventually, to zero) in the third composition interval, as evidenced by a disappearance of the SAXS peak and by a further decrease of the SAXS intensity in the relevant range of scattering angles at $\varphi \geq 0.5$ to well below the additivity (Fig. 3).

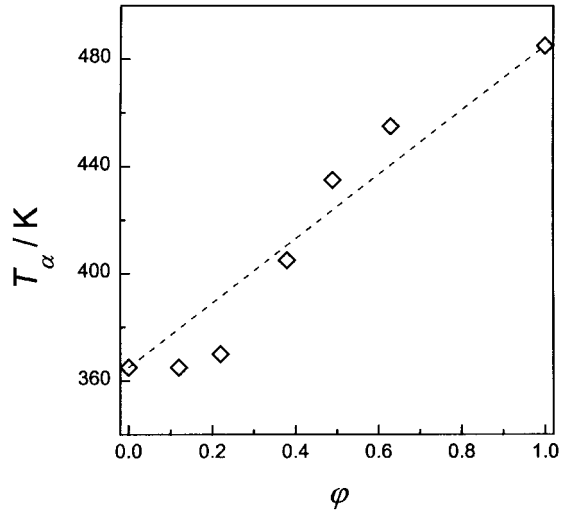

Fig. 5. Composition dependence of the α-relaxation temperature.

3.2. Thermal transitions

The unique feature of the plot of mechanical loss tangent vs. temperature for the neat CPU (Fig. 4) is the weak relaxation at the glass transition temperature of the SFT-rich microphase ($T_{g1} \approx 195$ K) which is followed by the much stronger, asymmetric relaxation spanning an unusually broad temperature interval and passing through a maximum at the apparent softening point of STF-rich microdomains ($T_{s1} \approx 365$ K). In case of the neat HPN, one observes the relatively weak sub-glass (β) relaxation around $T_{\beta 2} \approx 335$ K, and the major (α) relaxation with a peak at $T_{\alpha 2} \approx 570$ K and a low-temperature shoulder at $T_{\alpha' 2} \approx 485$ K (Fig. 4).

A feature common to all seq-IPNs is the essentially composition-invariant, weak low-temperature relaxation of the SFT microphase of the CPU (Fig. 4). In addition, the temperature values of the α-relaxation also remain nearly unchanged in the first composition interval $\varphi \approx 0.4$ (cf. Fig. 5 and Table 1). These observations are consistent with the concept of a microheterogeneous structure of seq-IPNs in this composition interval, comprising the SFT microphase of CPU swollen by the DCE, and the macrolattice of STF microdomains.

In contrast, a steady increase of T_α with φ in the composition interval above $\varphi \approx 0.4$ (Fig. 5) can be considered as

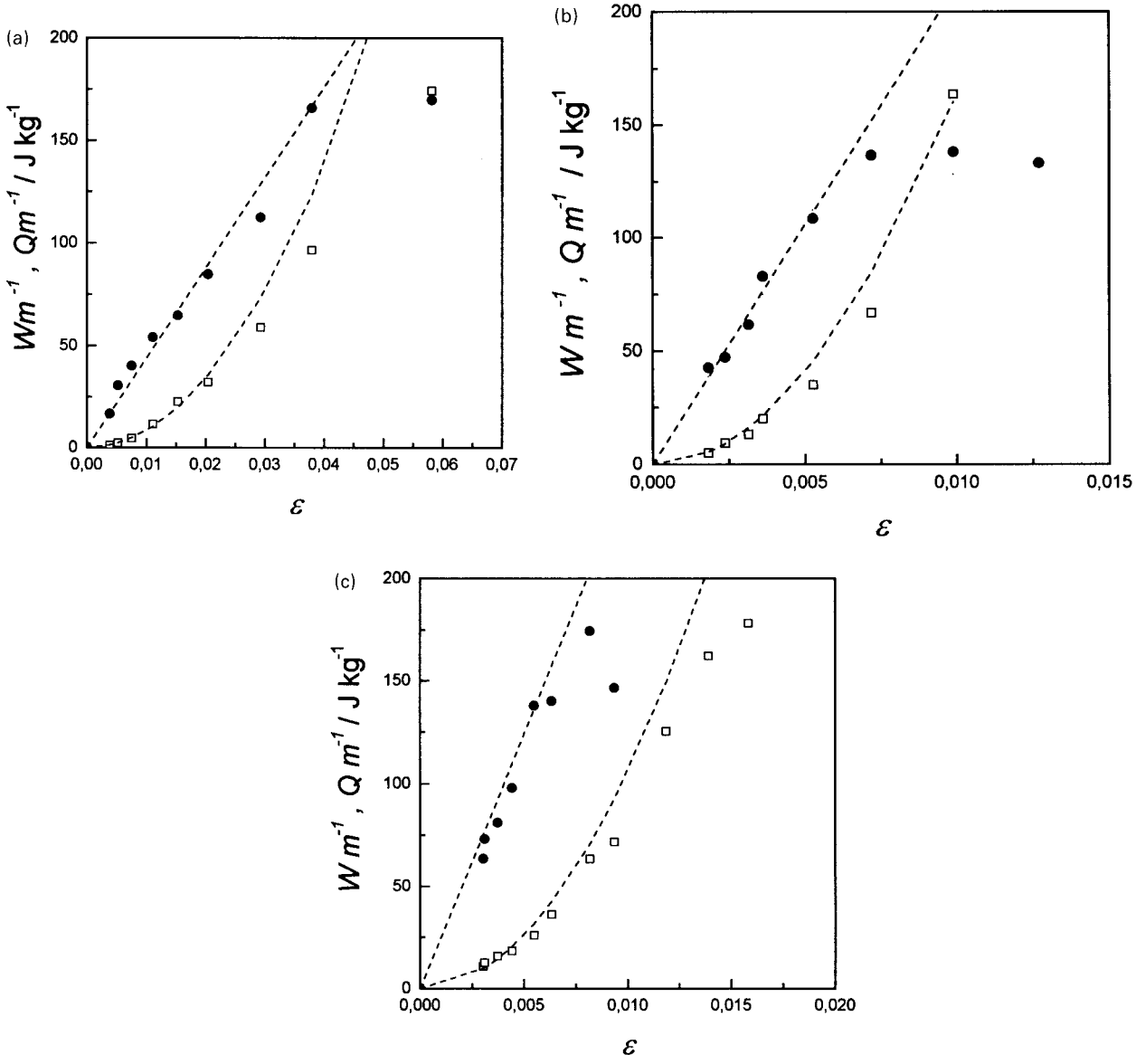

Fig. 6. Specific mechanical work (□) and specific heat effects (●) for (a) CPU, (b) HPN and (c) for CPU/HPN with (51/49) composition.

experimental evidence for a gradual decrease of the DMS of seq-IPNs due to the onset and further development of strong interactions between the excess of the molten DCE and the STF microdomains of the CPU. Here the relevant result is the "overshoot" of the experimental values of T_α above the linear additivity line (broken line in Fig. 5) which is the theoretical upper limit for compatible, "physical" polymer blends [24] (at least, for components obeying, approximately, the empirical rule, $\Delta c_p T_g \approx$ constant, where Δc_p is the specific heat capacity jump at T_g). It can, thus, be concluded that predominantly chemical interactions between molten DCE and the STF microdomains, complementing primary physical interactions (dilution), are the ones responsible for the observed cross-over to a more homogeneous phase morphology of seq-IPNs at $\varphi > 0.4$.

3.3. Thermoelastic properties

In the range of sufficiently small strains (i.e. below the apparent yield strain ϵ^*) the specific (per unit sample mass m) mechanical work (W/m) and specific heat effects (Q/m) for all studied systems quantitatively fitted the classical equations of the thermoelasticity of solids [25]

$$W/m = \frac{E\epsilon^2}{2\rho}; \tag{1a}$$

$$Q/m = \frac{E\alpha_L T\epsilon}{\rho} \tag{1b}$$

where E is the Young's modulus, α_L is the linear expansion coefficient, and ρ is the density. Fig. 6 illustrates the comparison of experimental and calculated data of W and

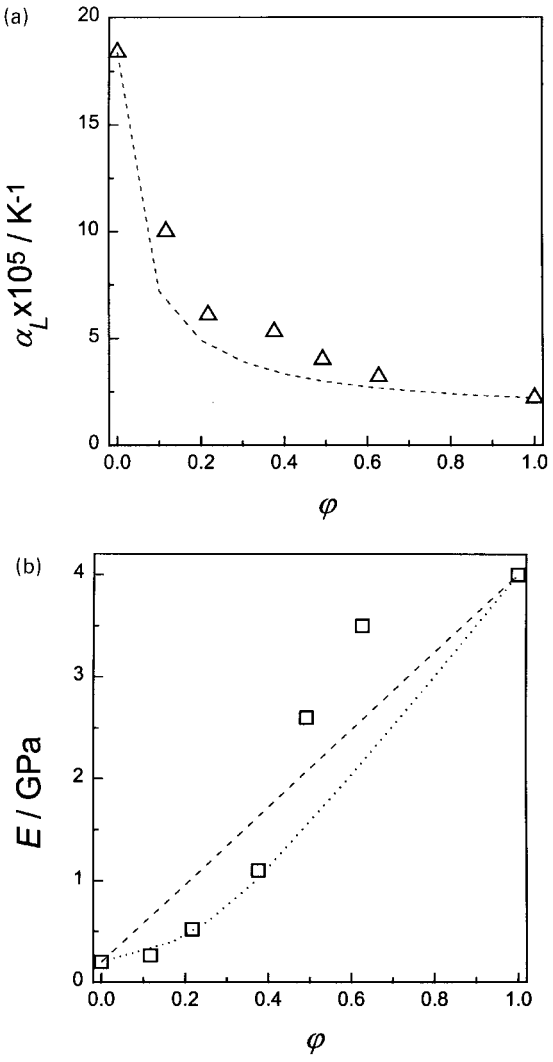

Fig. 7. Composition dependence of: (a) the linear thermal expansion coefficient and (b) Young's modulus.

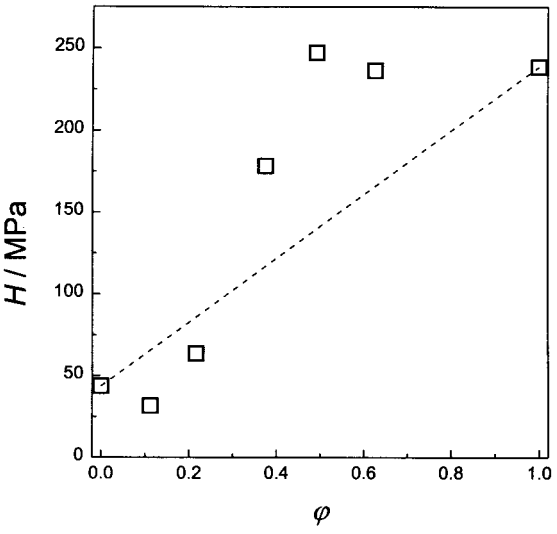

Fig. 8. Composition dependence of the microhardness.

Q as a function of strain for CPU, HPN and for the 51/49 CPU/HPN composition. As expected, the best-fit of E and α_L values (Table 1) increase and decrease, respectively, with increasing of the stiffer component content φ. The overall decrease of α_L with φ can be accounted for by any current theoretical approach available [26] such as the simple Turner equation [27] (broken line in Fig. 7a):

$$\alpha_L = \frac{\alpha_{L,1}B_1(1-\varphi) + \alpha_{L,2}B_2\varphi}{B_1(1-\varphi) + B_2\varphi}, \quad (2)$$

where $\alpha_{L,1}$ and B_1, and $\alpha_{L,2}$ and B_2 are the linear expansion coefficients and bulk moduli of CPU and HPN, respectively. However, no model can reproduce the apparent deviation around $\varphi \approx 0.4$ (by using Eq. (2), both components were assumed to have identical Poisson's coefficients ν_i; hence, bulk moduli $B_i = E_i/3(1-2\nu_i)$ could be substituted by the corresponding Young's moduli E_i).

Similarly neither can any theoretical model explain the observed S-shaped E vs. φ plot over the entire composition interval (Fig. 7b). Within the range $\varphi < 0.5$, the values of E were considerably below the theoretical upper bound (broken straight line in Fig. 7b) for the parallel model (i.e. the additivity of moduli) but somewhat higher than the theoretical lower bound for the series model (i.e. the additivity of reciprocal moduli or compliances). In this interval, the data could be fitted to the Budiansky equation [28],

$$\frac{1}{G} = \frac{1}{G_2} + \frac{(1-G_1/G_2)(1-\varphi)}{G + D(G_1 - G)}, \quad (3)$$

where G_1, G_2 are the shear moduli and $D = 2(4-5\nu)/15(1-\nu)$ (the best-fit, dotted line in Fig. 7b was calculated with Eq. (3) substituting G by $E/2(1+\nu)$ and assuming $\nu = \nu_1 = \nu_2 = 0.25$).

It is obvious that the unusually large overshoot of E values in the interval $\varphi \geq 0.5$ above the theoretical upper bound (broken straight line in Fig. 7b) cannot be accounted for by any theoretical model assuming composition-invariant structure and properties of each component in the neat state and in the seq-IPN, respectively. From the foregoing it can be inferred that the above basic assumption is approximately valid only below $\varphi \approx 0.5$ but it does not apply at higher HPN contents. In other words, we have to explain the observed effect by the increased contribution of strong chemical interactions between the components above $\varphi \approx 0.5$, resulting in the gradual development of a new structure with basically different thermoelastic properties.

3.4. Microhardness

Qualitatively, the plot of H vs. φ (Fig. 8) resembles the variation of E as a function of the composition shown in Fig. 7b. In fact, one observes negative and positive deviations from linear additivity (broken line in Fig. 8) below and above $\varphi \approx 0.4$, respectively. In line with the foregoing arguments, this behavior can be attributed to the continuously increasing contribution of strong

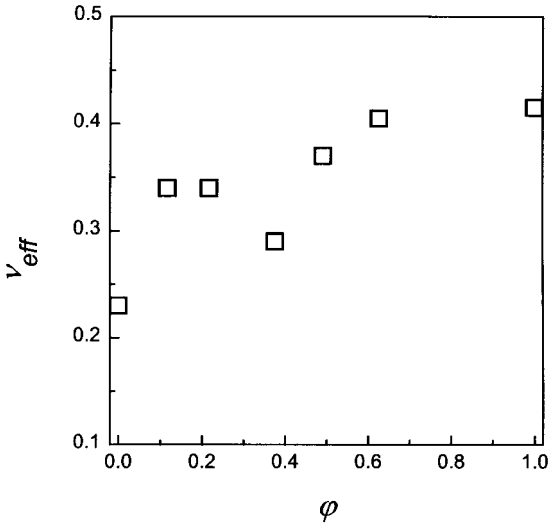

Fig. 9. Composition dependence of the effective Poisson coefficient.

chemical interactions between components of seq-PNs for $\varphi \geq 0.4$.

The observed similarity of composition dependence between E and H can be discussed in the light of Tabor's equation [29],

$$H \approx C\sigma_y, \tag{4}$$

where σ_y is the yield stress and C is the geometrical constant ($C = 3$ in the case of uniaxial compression). Approximating σ_y as the product of the Young's modulus E and the yield strain ϵ_y, and using the semi-empirical relationship [30] $\epsilon_y \approx (1 - 2\nu)/6(1 + \nu)$, one can derive from Eq. (4):

$$H \approx \frac{E(1 - 2\nu)}{2(1 + \nu)} \tag{4'}$$

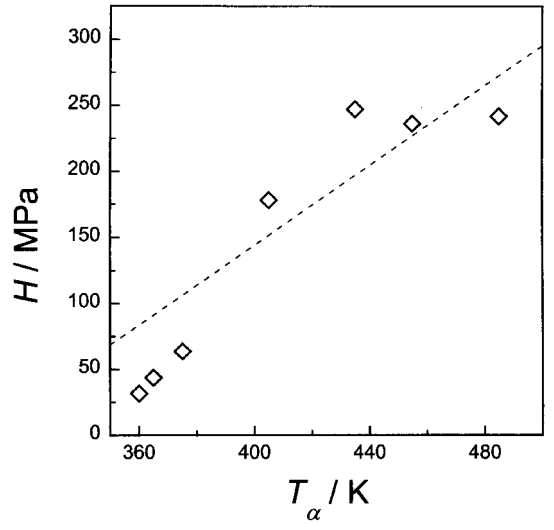

Fig. 10. Correlation between microhardness and the temperature of α-relaxation.

From this equation, both H and E should have a similar composition dependence for systems with essentially composition-invariant Poisson coefficients. In addition, the value of ν can be estimated from this equation. Fig. 9 shows the composition dependence of the "effective" value of ν as a function of φ. Here the identity of both quantities, E and C in the loading modes of uniaxial compression and of uniaxial stretching was assumed in the calculation. It seems worth noting at this point that the values of ν_{eff} below $\varphi \approx 0.4$ (Fig. 9) are reasonably close to $\nu = 0.25$ which ensured the best fit of the experimental Young's moduli E to the Budiansky equation (4) over the same composition interval (Fig. 7b).

The similar variation obtained for, both, T_α and H vs. φ (cf. Figs. 5 and 8) suggests the possibility to draw a correlation between the former quantities. In fact, assuming the excess enthalpy to be an alternative measure of the strength of a glassy quasilattice, the following relationship can be derived [12]:

$$H \approx C'\langle\Delta c_p\rangle(T' - T_g), \tag{5}$$

where C' is a numerical parameter, and $\langle\Delta c_p\rangle = c_{p,melt} - c_{p,glass}$ represents the mean difference between the specific heat capacities of a polymer in the melt and in the glassy state, respectively, in the temperature interval between the temperature of measurement T' and the glass transition temperature T_g.

Eq. (5) provides a reasonable explanation for the observed increasing correlation between H and T_α (cf. Table 1 and Fig. 10). However, the fit of the present data for full, seq-IPNs to the earlier empirical correlation for semi-IPNs of a similar nature [12] (broken line in Fig. 10) is not quantitative. This is not surprising, in so far as the fitting parameters C' and $\langle\Delta c_p\rangle$ in Eq. (5) should depend, in general, on the chemical nature of a glassy polymer. Moreover, it can be readily shown that the negative deviations of H for seq-IPNs in the interval $\varphi < 0.4$ are the obvious result of the contribution of mechanically weak SFT regions in the CPU. In fact, for these regions $T_{g1} < T'$. Hence, in view of Eq. (5) the contribution to the overall microhardness of the CPU can be neglected. In this respect, the SFT regions in the CPU are equivalent to the non-crystalline regions in a semi-crystalline polymer like polyethylene. In the latter case, the microhardness of the bulk specimen is directly proportional to its degree of crystallinity X (i.e. $H = XH_c$, where H_c is the microhardness of crystalline regions [31]). In the light of these considerations, the microhardness of the macrolattice of STF microdomains in the CPU can be estimated as $H_{STF} = H/W \approx 110$ MPa (here $W \approx 0.4$ is the mass fraction of STF fragments). It can be easily verified that the latter value fits much better to the expected correlation between H and T_α (broken line in Fig. 10). A similar correction can be also applied to other data points for seq-IPNs in the composition interval $\varphi < 0.4$.

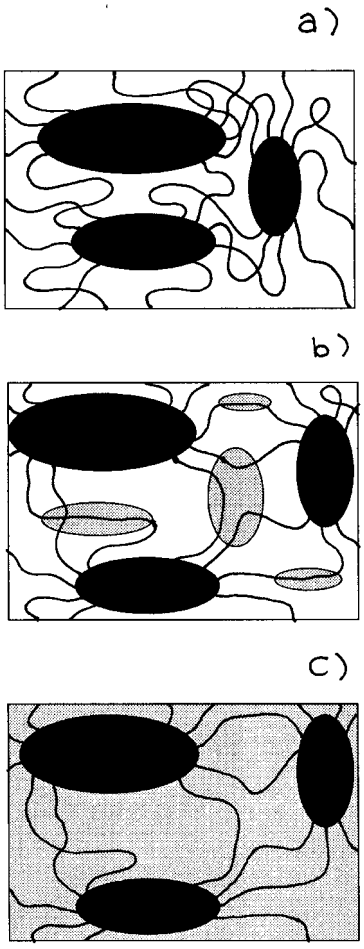

Fig. 11. Schematics of the local structure of: (a) CPU, (b) seq-IPNs ar $\varphi \leq 0.15$ and (c) $\varphi \geq 0.5$. Black areas: stiff microdomains of CPU; grey areas: HPN; continuous lines: soft chain fragments of CPU.

4. Conclusions

The characteristic dependence of L, DMS, T_α, E and H of a series of full, seq-IPNs upon composition has been explained according to the following model (Fig. 11). The maximum degree of the CPU swelling by molten DCE is reached already in the first composition interval. ($\varphi < 0.15$). However, the volume increment of the swollen CPU exceeds, by far, the actual content of the HPN within corresponding seq-IPNs. Hence, in the second composition interval ($0.15 \leq \varphi \leq 0.5$) only a relatively small fraction (i.e. of the order of $\varphi \approx 0.15$) of the available molten DCE was in a direct interaction with the expanded soft chain fragments of the CPU, whereas the remaining DCE simply filled the empty space created by swelling. This facilitated the accessability of unreacted functional groups at the periphery of stiff domains of the CPU to strong interactions with the excess of molten DCE. As a result, with increasing HPN content the sharp interface between components is gradually smearing out until a completely homogeneous structure is developed in the composition interval $\varphi > 0.5$. Predominantly, chemical interactions between the molten DCE and the STF microdomains of the CPU complementing primary physical interactions (dilution) are suggested to be responsible for the observed cross-over to a more homogeneous phase morphology of seq-IPNs at $\varphi > 0.4$. The latter conclusion requires experimental verification.

Acknowledgements

This work was supported by the DGICYT, Spain (Grant PB94-0049), and by the project INTAS-97-1936. Thanks are due to the Ministerio de Educacion y Cultura, Spain, for a sabbatical grant to V.P.P.

References

[1] Korshak VV, Pankratov VA, Ledovskaya AA, Vinogradova SV. Polym Sci Chem 1978;16:1697.
[2] Omelchenko SI, Kadurina TI. Modified polyurethanes, Kiev: Naukova Dumka, 1983 in Russian.
[3] Privalko VP, Kramarenko VYu, Maslak YuV, Rosovitsky VF. Colloid Polym Sci 1993;271:322.
[4] Kramarenko VYu. PhD thesis. Institute f Macromolecular Chemistry, National Academy of Sciences of Ukraine, Kiev, 1993 (in Russian).
[5] Hamerton I, editor. Chemistry and technology of cyanate ester resins Chapman & Hall, 1994.
[6] Sergeeva LM, Semenovich GM, Karabanova LV, Lipatova TE, Lipatov YuS. Dokl Akad Nauk SSSR 1986;288:1134.
[7] Fainleib AM, Novikova TI, Shantalii TA, Sergeeva LM. Vysokomol Soed 1992;B33:60.
[8] Brovko AA, Fainleib AM, Shantalii TA, Sergeeva LM, Davidenko VV. Vysokomol Soed 1994;A36:1132.
[9] Bartolotta A, DiMarco G, Lanza M, Carini G, D"Angelo G, Tripodo G, Fainleib A, Slinchenko EA, Privalko VP. Adhesion 1997;64:269.
[10] Bartolotta A, DiMarco G, Lanza M, Carini G, D"Angelo G, Tripodo G, Fainleib A, Slinchenko EA, Shtompel VI, Privalko VP. Polym Engng Sci 1999.
[11] Bartolotta A, DiMarco G, Carini G, D"Angelo G, Tripodo G, Fainleib A, Privalko VP. J Non-Cryst Solids 1998;235-237:600.
[12] Balta Calleja FJ, Privalko EG, Fainleib AM, Shantalii TA, Privalko VP. Submitted for publication.
[13] Semenovich GM, Khramova TS. IR and NMR spectroscopy of polymers, Handbook on physical chemistry of polymers. Kiev: Naukova Dumka, 1985 in Russian.
[14] Lipatov YuS, Shilov VV, Gomza YuP, Kruglyak NE. X-Ray methods of characterization of polymer systems, Kiev: Naukova Dumka, 1982 in Russian.
[15] Oranskaya EI. PhD thesis, Institute of Macromolecular Chemistry, National Academy of Sciences of Ukraine, 1991 (in Russian).
[16] Mirontsov LI. PhD thesis, Institute of Macromolecular Chemistry, National Academy of Sciences of Ukraine, Kiev, 1987.
[17] Tregub AI. PhD thesis, Institute of Macromolecular Chemistry, National Academy of Sciences of Ukraine, Kiev, 1990.
[18] Tregub AI, Privalko VP, Kilian H-G, Marom G. Appl Composite Mater 1994;1:167.
[19] Balta Calleja FJ. Adv Polym Sci 1985;66:117.
[20] Santa Cruz C, Balta Calleja FJ, Zachmann HG, Stribeck N, Asano T. J Polym Sci Phys 1991;29:819.
[21] Privalko VP, Shapoval RL, Usenko AA, Oranskaya EI. Polym Engng Sci 1997;37:983.
[22] Oberth AE. Rubber Chem Tech 1990;63:56.

[23] Pogosyan MN, Pankratov VA, Zaplishnyi VN, Matsoyan SG. Polytriazines, Erevan, 1987 (in Russian).
[24] Couchman PR. Macromolecules 1980;13:1272.
[25] Godovsky YuK. Thermophysical properties of polymers, Berlin: Springer, 1992.
[26] Privalko VP, Novikov VV. The science of heterogeneous polymers, Chichester: Wiley, 1995.
[27] Turner PS. Res Natl Bur Stand 1946;37:239.
[28] Budiansky B. Mech Phys Solids 1965;13:223.
[29] Tabor D. The hardness of metals, Oxford: Clarendon Press, 1951.
[30] Kozlov GV, Sanditov DS. Anharmonic effects in physical and mechanical properties of polymers, Novosibirsk: Nauka, 1994 in Russian.
[31] Balta Calleja FJ. Trends Polym Sci 1994;2:419.